

First-principles approach to spin-orbit coupling in dilute magnetic semiconductors

G. Theurich* and N. A. Hill

Materials Department, University of California, Santa Barbara, California 93106-5050

(Received 16 April 2001; revised manuscript received 5 April 2002; published 30 September 2002)

We describe the implementation of a spin-polarized fully relativistic plane wave pseudopotential density functional method. Using the method, we compare the calculated electronic band structures of hypothetical ferromagnetic zinc blende structure MnAs and MnSe within the scalar-relativistic and fully relativistic pseudopotential approximations. We extract the conduction band and valence band exchange constants and extrapolate to the low concentration limit following a simple mean field approximation. Finally we investigate how strongly the exchange constants are affected by the spin-orbit term and provide a computational justification for extracting these constants from scalar-relativistic calculations.

DOI: 10.1103/PhysRevB.66.115208

PACS number(s): 71.20.Be, 71.70.Ej, 71.70.Gm

I. INTRODUCTION

Dilute magnetic semiconductors (DMS's) are by now a well established class of materials. Conventional manganese-doped DMS's are based on II-VI materials such as ZnSe or ZnTe, in which very high manganese concentrations can be achieved. In fact thin layers of pseudomorphic zinc blende MnSe can be stabilized artificially by means of nonequilibrium epitaxial growth techniques despite the fact that bulk MnSe crystallizes in the NaCl structure.^{1,2} In contrast bulk MnAs crystallizes in the hexagonal NiAs structure and has not been stabilized in the zinc blende structure.³ Nevertheless, DMS's based on III-V materials such as GaAs or InAs have recently been fabricated by means of low-temperature molecular beam epitaxy with manganese concentrations reaching 10%.^{4,5}

Despite the large number of experimental and theoretical works dedicated to the electronic and magnetic properties of DMS's there are many questions that remain unanswered.^{1,6} For example a recently proposed mean-field model received a significant amount of attention since it allows the quantitative prediction of the Curie temperature—a parameter of utmost technological interest—for a variety of ferromagnetic semiconductors.^{7,8} However, some of the most important parameters entering the mean-field model, the so-called conduction band and valence band exchange constants $N\alpha$ and $N\beta$ are only known for a limited number of relevant materials⁷.

In principle it is straightforward to extract $N\alpha$ and $N\beta$ from appropriate band structure calculations.⁹ However the experimental $N\beta$ is properly defined as the exchange constant for the Γ_8 level of the host semiconductor, implying that an exact theoretical treatment of the exchange constants needs to take the effect of spin-orbit coupling into account. Nevertheless, band structure calculations that are used to determine the exchange constants in DMS materials are usually carried out within the scalar-relativistic approximation.

The results presented in this paper are the first application of a recent implementation of spin-orbit coupling within the *ab initio* pseudopotential scheme of density functional theory to magnetic systems. Our motivation for including spin-orbit coupling explicitly in our study comes from the fact that there are a number of spin-dependent effects in semiconduc-

tors that are governed by spin-orbit coupling. Examples are the spin-relaxation of conduction electrons^{10,11} and anisotropic superexchange and weak ferromagnetism.¹²⁻¹⁴ Very recently anisotropic ferromagnetic coupling in DMS's has also been attributed to the effect that spin-orbit coupling has on the valence band in these materials.^{7,8}

A brief review of the method for non-spin-polarized systems¹⁵ is given in Sec. II A of this paper, followed in Sec. II B by details on generalization of the local spin density approximation to include spin-orbit coupling in spin-polarized systems. Symmetry considerations are discussed in Sec. II C.

In Sec. III we apply the scalar- and fully relativistic pseudopotential methods to hypothetical ferromagnetic zinc blende MnAs and MnSe. This allows us to study the interplay between spin-orbit coupling and exchange interaction in these materials. We find that the generally accepted Kondo-like form of the *p-d* interaction cannot account for exact levels of the relativistic bands structure. However, the quantitative effect is small compared to the large exchange splitting and affects the exchange constants little.

II. COMPUTATIONAL TECHNIQUES**A. Spin-orbit coupling in the pseudopotential scheme**

The *ab initio* pseudopotential method¹⁶⁻¹⁸ has become a standard tool in many areas of electronic structure calculation. Even magnetic compounds containing 3*d* transition metal ions now lie in the realm of the plane wave pseudopotential approach of density functional theory.^{19,20} In order to obtain high precision results it is necessary to include relativistic effects when calculating the electronic structure of materials containing third row elements.²¹ Hence it is now standard procedure to create scalar-relativistic pseudopotentials that include the kinematic relativistic effects (mass-velocity and Darwin term) from the fully relativistic all-electron solution of the atom.²²⁻²⁶

In the scalar relativistic approximation, however, the spin-orbit interaction is only effectively taken into account by the construction of *j*-averaged pseudopotentials for each angular momentum *l*. Consequently no spin-orbit splittings are

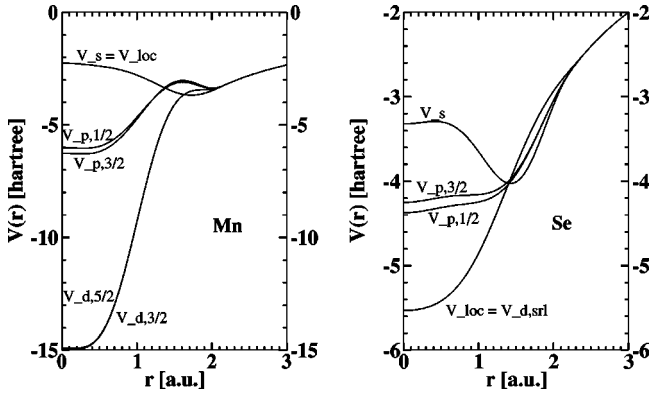


FIG. 1. The ionic pseudopotentials $V_{l\pm 1/2}(r)$ and the local part V_{loc} for manganese (left) and selenium (right).

present in the resulting band structure. For cases where these splittings play a major role it is mandatory to include spin-orbit coupling explicitly.

For periodic systems the spin-orbit interaction is appropriately written in the form²⁷

$$H_{SO} = \frac{\hbar}{4m_0^2 c^2} (\vec{\nabla} V \times \vec{p}) \cdot \vec{\sigma}. \quad (1)$$

It is strongest close to the ion cores where the gradient of the potential is largest. However, this is the region which is covered by the pseudopotentials. Thus it is impossible to add the spin-orbit effect *a posteriori* to the scalar-relativistic pseudopotential results; instead the pseudopotentials themselves must account for spin-orbit coupling. For the nonlocal pseudopotential scheme it has been shown by Kleinman that all relativistic effects are captured to order α^2 , where α is the fine structure constant, when the pseudopotential components are constructed from the major component of the fully relativistic solution of the atomic problem.²⁸ Naturally, the pseudopotentials become dependent on the total angular momentum j and operate in orbital and spin space. The details of the implementation of j -dependent pseudopotentials for non-spin-polarized systems have been given in an earlier paper¹⁵ so we do not repeat them here. However, we point out that the construction of the pseudopotential operator automatically leads to the correct symmetrization of the spin-orbit term in the crystal environment. All solid state calculations reported in this paper were carried out using SPINOR, our code capable of including spin-orbit coupling for spin-polarized systems, which is freely available²⁹ under the GNU public license.

In Fig. 1 we show our ionic pseudopotentials for manganese and selenium that were created following the fully relativistic procedure, within the Troullier-Martins scheme.²⁵ The core radii for all components of the manganese pseudopotential were set at 2.20 a.u. and the s component served as the local potential in the Kleinman-Bylander transformation.³⁰ For the selenium components 2.30 a.u. was chosen for the s and p components and 2.50 a.u. for the d component, which was the local component in this case. Due to a non-negligible overlap of the valence electrons with the core

charge density we applied nonlinear core corrections³¹ with a partial core radius of 0.70 a.u. to the manganese pseudopotential.

B. General local spin density approximation

In addition to the use of j -dependent pseudopotentials, extensions also have to be made to the conventional density functional formalism in order to treat spin-orbit coupling fully relativistically. The details of how to implement spin-orbit coupling in the plane wave pseudopotential method for a self-consistent treatment of non-spin-polarized systems have been given previously by the authors.¹⁵ Here we describe the further developments required when spin-orbit coupling is included in the calculation of *spin-polarized* systems. In this case an additional spin-dependent term is present in the Hamiltonian, arising from the exchange-correlation term of spin density functional theory (SDFT) (Refs. 32–34)

$$H_{xc} = \frac{\delta E_{xc}[n, \vec{m}]}{\delta(n, \vec{m})}. \quad (2)$$

Here n and \vec{m} are the fundamental variables of SDFT and stand for the electron density and spin polarization, respectively. Usually H_{xc} is approximated by the local spin density approximation (LSDA). For the special case of collinear spin polarizations, the exchange-correlation term does not couple the spin degree of freedom to the orbital motion. Then each Kohn-Sham function is automatically an eigenstate of one of the components of the Pauli spin operator $\vec{\sigma}$, which is typically chosen to be the z component.

As is well known, the spin-orbit term of Eq. (1) mixes the spin eigenstates. For non-spin-polarized systems, i.e., for $\vec{m} = 0$ at every point in space, this does not cause any complications. However, for spin-polarized systems the spin-polarization for each individual Kohn-Sham function ψ_i needs to be expressed in the general form

$$\vec{m}_i(\vec{r}) = \psi_i^*(\vec{r}) \vec{\sigma} \psi_i(\vec{r}). \quad (3)$$

It is clear that the sum over all occupied states can produce a noncollinear total spinpolarization \vec{m} and the usual collinear assumption fails. It has been shown that the generalization of H_{xc} to noncollinear spin polarizations is straightforward in the case of the local density approximation.^{34–36} The exchange-correlation term can be written in the general local spin density approximation (GLSDA) as

$$H_{xc} = a_{xc} 1_{2 \times 2} + \vec{b}_{xc} \cdot \vec{\sigma}, \quad (4)$$

where

$$a_{xc}(\vec{r}) = \frac{\delta E_{xc}[n, \vec{m}]}{\delta n(\vec{r})} = \frac{\delta E_{xc}[n, m]}{\delta n(\vec{r})} \quad (5)$$

and

$$\vec{b}_{\text{xc}}(\vec{r}) = \frac{\delta E_{\text{xc}}[n, \vec{m}]}{\delta \vec{m}(\vec{r})} = \frac{\delta E_{\text{xc}}[n, m]}{\delta m(\vec{r})} \hat{m}(\vec{r}) . \quad (6)$$

Here $\hat{m}(\vec{r})$ denotes a unit vector in the direction of the spin polarization at point \vec{r} . Since at each point we can rotate the reference system in the direction of the spin polarization, it follows that the functional derivatives of the exchange-correlation energy with respect to the electron density and spin polarization, respectively, are equivalent to the expressions of conventional LSDA. We use the parametrization by Perdew and Zunger³⁷ to approximate the density and polarization dependent exchange-correlation energy.

C. Symmetries

We pointed out in the last section that without the effect of spin-orbit coupling it is always possible to separate the spin polarized problem according to the z component of the electron's spin. The up- and down-spin problems can be solved independently, coupled only by the requirement of overall self-consistency. Without spin-orbit coupling the spin polarization direction is completely arbitrary and no coupling to the lattice exists. Consequently the Hamiltonian reflects the symmetry of the full space group of the crystal, and both the electron density $n(\vec{r})$ and the magnitude of the spin polarization $m(\vec{r})$ can be obtained by symmetrization from a reduced set of states in the Brillouin zone.³⁸ Note further that the complex conjugate operation K_0 also enters the symmetry group, resulting in a twofold degeneracy of states with opposite sign of their Bloch wave vectors. Interestingly, since K_0 does not invert the spin quantum number of the state, this symmetry holds for any collinear spin polarization even for magnetic orders that are not invariant under time reversal such as ferromagnetically ordered states.

The presence of the spin-orbit term, however, prevents the separation of the problem into up and down components. Then each symmetry operation that is applied to the lattice also affects the spin polarization. Thus, in general the number of symmetry operations will be reduced from the full space group of the crystal to those that preserve the spin polarization at the same time. For clarity we adopt a notation similar to that of spin space groups³⁹ (SSG's) and write an arbitrary symmetry operation as

$$\{\alpha_S | \alpha_R | \vec{\tau}\}, \quad (7)$$

where α_S and α_R are general 3×3 rotation matrices and $\vec{\tau}$ is a spatial translation vector. The transformations are defined by their action on the electron density

$$\{\alpha_S | \alpha_R | \vec{\tau}\} n(\vec{r}) = n[\alpha_R^{-1}(\vec{r} - \vec{\tau})] \quad (8)$$

and spin polarization

$$\{\alpha_S | \alpha_R | \vec{\tau}\} \vec{m}(\vec{r}) = \alpha_S \vec{m}[\alpha_R^{-1}(\vec{r} - \vec{\tau})]. \quad (9)$$

The action on a two-component spinor $\psi(\vec{r})$ is given by

$$\{\alpha_S | \alpha_R | \vec{\tau}\} \psi(\vec{r}) = R^{1/2}(\alpha_S) \psi[\alpha_R^{-1}(\vec{r} - \vec{\tau})], \quad (10)$$

TABLE I. Point group operations for zinc blende structure with net magnetization along [001].

K'	1	1	1	1	K	K	K	K
α_S	1	C_{2z}	C_{4z}	C_{4z}^{-1}	C_{2x}	C_{2y}	C_{2xy}	C_{2xy}^{-}
α_R	1	C_{2z}	C_{4z}^{-1}	C_{4z}	C_{2x}	C_{2y}	σ_{xy}	σ_{xy}^{-}

where $R^{1/2}$ is the 2×2 spin rotation matrix corresponding to the rotation α_S . For a general rotation with Euler angles α , β , and γ the spin rotation matrix is⁴⁰

$$\begin{pmatrix} e^{-(1/2)i\alpha} \cos \frac{1}{2}\beta e^{-1/2i\gamma} & -e^{-(1/2)i\alpha} \sin \frac{1}{2}\beta e^{+1/2i\gamma} \\ e^{+(1/2)i\alpha} \sin \frac{1}{2}\beta e^{-1/2i\gamma} & e^{+(1/2)i\alpha} \cos \frac{1}{2}\beta e^{+1/2i\gamma} \end{pmatrix}. \quad (11)$$

The restrictions introduced by the coupling of the spin and orbital degrees of freedom can only be satisfied if we require $\alpha_S = \alpha_R$ for every proper rotation in the symmetry group.⁴¹ However, in the case of an improper rotation α_R we note that the spin polarization is unchanged under spatial inversion J due to its axial nature, and thus $\alpha_R = J\alpha_S$.

We note further that complex conjugation no longer represents an allowed symmetry operation when the spin-orbit term is included. However, as is well known, the spin-orbit term is invariant under the action of the time reversal operator

$$K = -i\sigma_y K_0. \quad (12)$$

This leads to Kramer's degeneracy in the case of paramagnetic band structures. However, for spin-ordered systems the isolated operation K is not a symmetry operation either since it leads to the equality $\vec{m}(\vec{r}) = -\vec{m}(\vec{r})$ at all points in space. On the other hand if the time-reversal operation is coupled with certain spatial symmetry operations we can construct allowed transformations. In order to illustrate this fact, picture a collinear ferromagnetic structure. Then a rotation by 180° along an axis perpendicular to the magnetization axis is not a symmetry operation even if it leaves the chemical crystal unchanged. But if the same rotation is followed by the time-reversal operation the original magnetization is restored.

The underlying symmetry of the chemical lattices studied in this work is that of the cubic T_d point group which contains the 24 spatial rotations $1, 8C_3, 3C_2, 6\sigma_d$, and $6S_4$. Then, for the scalar-relativistic calculations, the general point group operation has the form $\{\mathbf{1} | \alpha_R | 0\}$, where α_R stands for any of the 24 rotations in T_d . For the fully relativistic case, however, the general point group operations take on the form

$$K' \{\alpha_S | \alpha_R | 0\}, \quad (13)$$

where $\alpha_S = J\alpha_R$ or $\alpha_S = \alpha_R$ depending on whether the rotation α_R contains spatial inversion or not. The operation K' refers to either identity or the Kramers' operator defined in Eq. (12). The resulting tetragonal point group for the case with spin polarization along the [001] direction only has eight symmetry operations which are given in Table I.

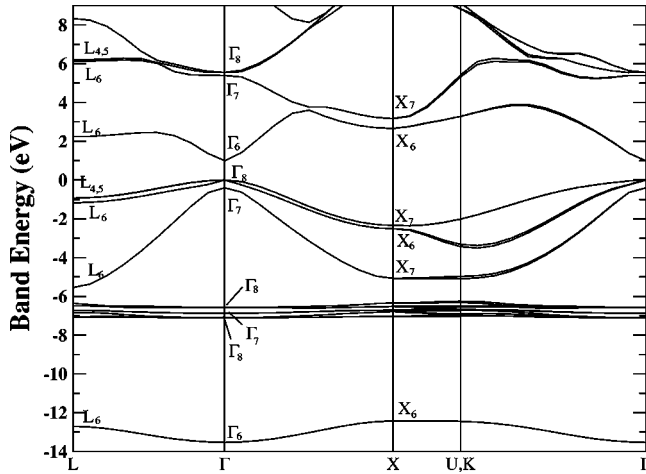


FIG. 2. Fully relativistic band structure of ZnSe.

III. RESULTS AND DISCUSSION

In this section we apply the scalar-relativistic and fully relativistic pseudopotential approximations to the cases of zinc blende structure MnSe and MnAs. For both materials we consider the ferromagnetic spin alignment. We note that although MnSe can be stabilized in the zinc blende structure it does not exhibit ferromagnetism but rather orders antiferromagnetically.^{2,42} DMS materials based on II-VI compounds, however, show paramagnetic behavior.¹ Bulk MnAs on the other hand is more difficult to stabilize in the zinc blende structure and only low concentrated III-V-DMS's have been grown successfully.⁴ This class of DMS's orders ferromagnetically with transition temperatures up to 110 K.⁵ Zinc blende MnSe and MnAs can thus be viewed as the high concentration limit of the appropriate DMS material. In the case of MnSe the enforced ferromagnetic order models the effect of an external magnetic field which produces a finite magnetization. For MnAs it corresponds to the actual LSDA ground state of the high concentration limit.

A. A benchmark study; fully relativistic ZnSe

First, as a test case of our implementation, and as a benchmark to compare our later results for ferromagnetic materials, Fig. 2 shows the fully relativistic band structure of non-spin-polarized zinc blende ZnSe obtained using j -dependent pseudopotentials for zinc (not shown) and selenium (Fig. 1). This is, to our knowledge, the first published relativistic band structure calculation of ZnSe based on the *ab initio* pseudopotential scheme. Chelikowsky and Cohen previously determined the relativistic band structure of ZnSe based on the empirical pseudopotential method, excluding the Zn $3d$ states from the valence.⁴³

We find that the split-off hole band is clearly separated from the light hole (lh), heavy hole (hh) degeneracy at Γ . Further the lh , hh degeneracy, which is present along the L - Γ - X line for scalar-relativistic calculations, is lifted by the spin-orbit coupling term. The calculated spin-orbit splitting of the top of the valence band at the Brillouin zone center of 0.41 eV is reasonably close to the experimentally available value of 0.42 eV.^{44,45} Also, the splitting of 0.24 eV at the L

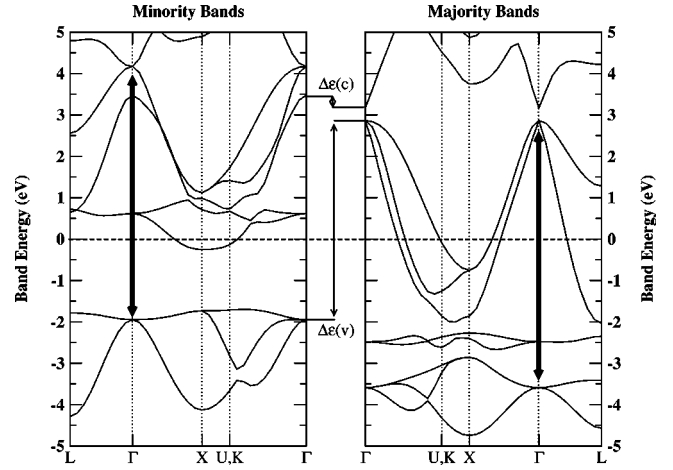


FIG. 3. Band structure for majority and minority spin states of hypothetical ferromagnetic zinc blende MnAs at a lattice constant of 5.65 Å. The highlighted splittings are discussed in the text.

point compares well with experimental data that gives a range between 0.20 and 0.30 eV for this splitting.^{44,45} It is interesting to note the lifting of the threefold degeneracy of the zinc t_2 d states, whereas the d states of e symmetry seem to be unaffected by spin-orbit coupling.

Finally we observe that the band gap for relativistic ZnSe is halved compared to the value we obtain in the non-relativistic approximation. This reduction of the band gap is due to well documented relativistic band shifts which are larger for the antibonding bottom of the conduction band than for the bonding top of the valence band.⁴⁶ In addition the spin-orbit splitting of the valence band top further reduces the band gap in the fully relativistic result.

B. Scalar-relativistic pseudopotential results for MnAs and MnSe

Figures 3 and 4 show our calculated band structures for ferromagnetic zinc blende MnAs and MnSe, respectively, using j -averaged scalar-relativistic pseudopotentials. The lattice

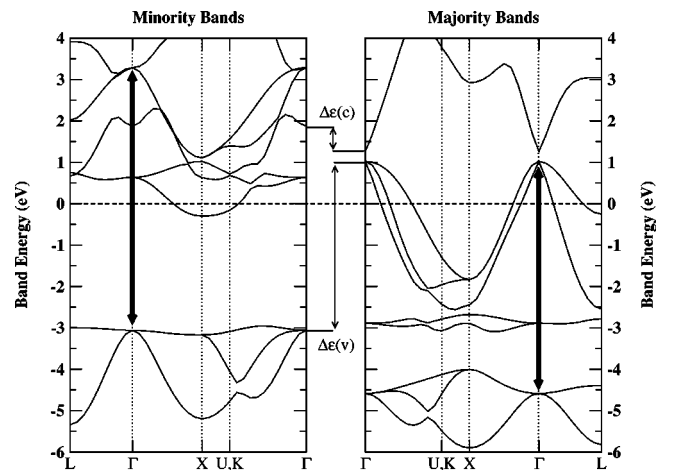


FIG. 4. Band structure for majority and minority spin states of hypothetical ferromagnetic zinc blende MnSe at a lattice constant of 5.65 Å. The highlighted splittings are discussed in the text.

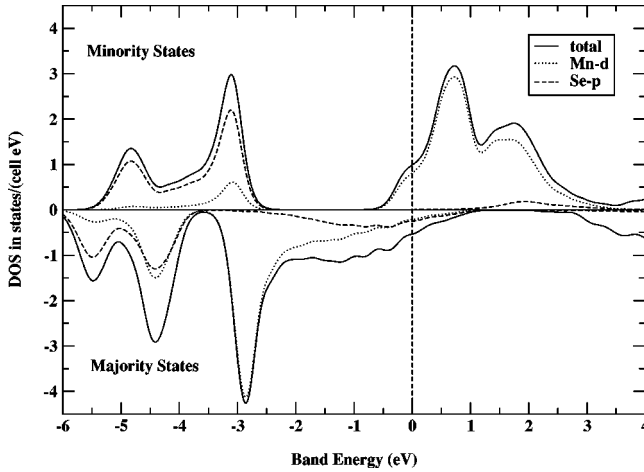


FIG. 5. Total and projected density of states for majority and minority spin states of hypothetical ferromagnetic zinc blende MnSe at a lattice constant of 5.65 Å.

constant has been chosen to match the experimental value of 5.65 Å for GaAs and ZnSe, so as to simulate the experimental situation where these substrates are often used. All calculations have been carried out for the ideal zinc blende structure, and possible distortions have been neglected. The distinction between minority and majority bands is given by the z component of the electron spin, which in the scalar-relativistic approximation remains a good quantum number. The striking similarity of the two band structures emphasizes the fact that the underlying ionic potentials in MnAs and MnSe are very similar. However, the position of the Fermi level, which is determined by the number of electrons per formula unit, is quite different for MnAs and MnSe with respect to the majority spin states. For MnAs the Fermi level lies right in the center of the upper most majority valence band manifold whereas for MnSe, which has one additional electron per formula unit, it resides closer to the top of the same valence band. The position of the Fermi level with respect to the minority states is almost identical in both materials, only barely cutting through the bottom of the lowest unoccupied band, leading to an almost half-metallic electronic structure for MnAs as has been reported earlier.³

The main features of the overall band structures for both MnAs and MnSe are determined by the energetic position of the spin-polarized manganese d states and their influence on the cation p bands, driven by a strong p - d hybridization interaction. To analyze this in more detail we show the projected density of states for MnSe in Fig. 5. The density of states for MnAs is very similar to that of MnSe (as one can imagine from the similar band structures) and is not shown here.

In compliance with Hund's first rule we find that the exchange interaction splits the strongly localized manganese d states into a group of occupied majority states and a group of unoccupied minority states. In addition, the projected density of states of Fig. 5 reveals that some of the occupied valence states in MnSe have strong Se- p character. As a result of this hybridization small spin polarization is induced on the Se sites. Furthermore the antibonding top of the majority va-

lence band is pushed upwards by the hybridization, away from the bonding states at around -5 eV. The hybridization interaction is smaller for the minority states since the exchange interaction raises the minority d states several eV above the valence band top. Nevertheless, even for the minority states, p - d hybridization is evident in the projected density of states, leading to a small downwards shift of the minority valence band. Thus the exchange splitting of the manganese d states introduces a sizable splitting of the mostly p -like valence band in MnAs and MnSe that is opposite in sign, meaning that the majority p bands lie higher in energy than the minority p bands. The relevant splittings are labeled $\Delta\varepsilon(v)$ in Figs. 3 and 4. The thick arrows at Γ highlight the states that strongly interact via hybridization.

Figures 3 and 4 further show a small splitting of the s -like conduction band at Γ labeled $\Delta\varepsilon(c)$. In contrast to the p -like valence states we find the splitting of the conduction band to be positive. To understand why s - and p -like states are affected differently by the exchange splitting of the manganese d states, it is important to realize that the s -like states at Γ cannot hybridize with states of d symmetry. Thus it is direct Coulomb exchange alone that leads to the observed conduction band exchange splitting.

Despite their different nature, it is possible and convenient to describe the s - d and p - d interactions in DMS materials in a formally similar fashion. Since the s - d interaction is a result of direct Coulomb exchange it is conveniently written in the Kondo form

$$H_{s-d} = -N_0\alpha\vec{S}\cdot\vec{s}, \quad (14)$$

where N_0 is the number of unit cells in the crystal, α is the exchange integral, and \vec{S} and \vec{s} are the spin operators of the manganese d states and the s -like conduction band electrons, respectively. Schrieffer and Wolff have shown that the hybridization interaction between localized impurity levels and the delocalized host states can also be transformed into a Kondo-like form,⁴⁷

$$H_{p-d} = -N_0\beta\vec{S}\cdot\vec{s}. \quad (15)$$

The Schrieffer-Wolff transformation relates the effective exchange integral (β), which will be negative in general, to the matrix elements of the interaction potential between the bands of the crystal.

Following Eqs. (14) and (15) it is straightforward to extract the exchange constants $N_0\alpha$ and $N_0\beta$ from the bulk band structures.⁹ Since all spins are collinear in our scalar-relativistic calculation, $\Delta\varepsilon(c)$ and $\Delta\varepsilon(v)$ simply need to be divided by half of the total spin polarization given in units of Bohr magnetons. The results that we obtain from our scalar-relativistic calculations for MnAs and MnSe are compiled in Table II and will be discussed in more detail in the following section. It is worth pointing out once more that the present results for the exchange constants are derived from calculations in the high concentration limit and as such are not directly comparable to the values obtained by Sanvito *et al.* from a low concentration fit of large super cell calculations.⁴⁸

TABLE II. Spin-polarization and exchange constants for MnAs and MnSe.

	$ M $ (μ_B)	$N_0\alpha$ (eV)	$N_0\beta$ (eV)
MnAs scalar relativistic	3.44	0.18	-2.82
MnSe scalar relativistic	4.42	0.28	-1.85

C. Mean-field interpolation

Within a simple mean-field approximation it is possible to extrapolate the high concentration results of the last section to the experimentally accessible low concentration limit. In the mean-field model, the interaction between the delocalized carriers and the localized manganese d moments is approximated by an interaction with an effective moment of strength $x\langle S \rangle$, where x is the effective manganese concentration and $\langle S \rangle$ is the average manganese d moment. Taking the average moment along the z direction, the two interaction terms simplify to

$$H_{s-d} = -N_0\alpha x\langle S \rangle s_z \quad (16)$$

and

$$H_{s-p} = -N_0\beta x\langle S \rangle s_z. \quad (17)$$

In addition to the interactions of Eqs. (16) and (17) a complete description of the spin interactions in semiconductors must also contain the spin-orbit term. Furthermore, if an external magnetic field is applied, as is the case for the paramagnetic II-VI DMS materials, the Zeeman and Landau splittings must, in principle, also be taken into account. However, for wide-gap host materials such as ZnSe, both the effective electron mass and g factor are reasonably close to 1. As a result, the Landau and Zeeman splitting can be neglected leading to only two competing spin-dependent terms in the Hamiltonian, exchange and spin-orbit coupling.

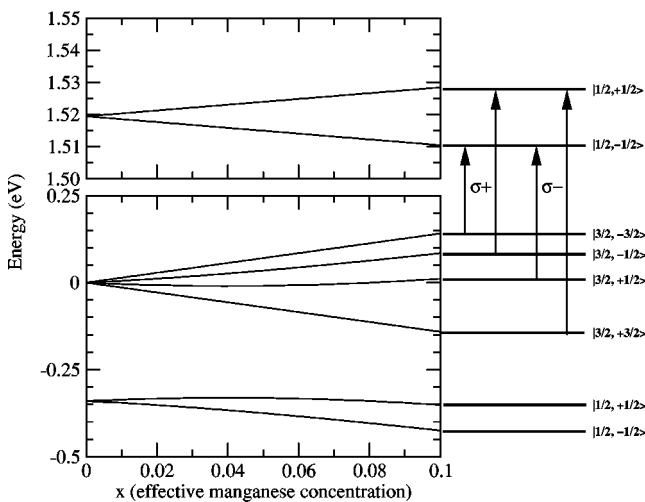


FIG. 6. Splitting of the $\text{Ga}_{1-x}\text{Mn}_x\text{As}$ valence and conduction band edges as a function of manganese concentration x , assuming a manganese polarization of 100% and using the computed spin polarization from Table II. The optical transitions between the valence and conduction band are also shown for circularly polarized light.

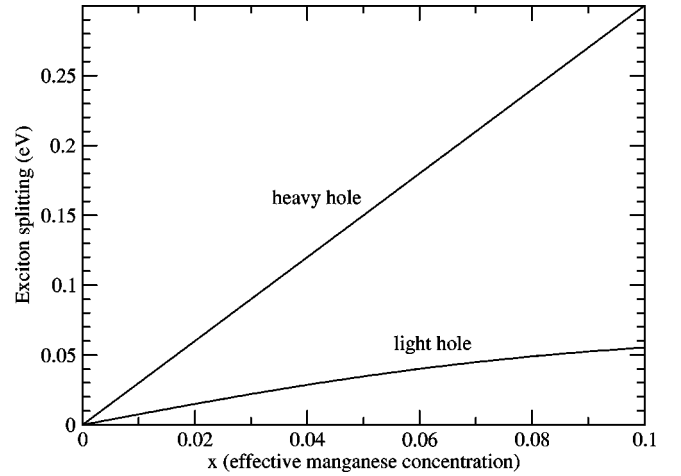


FIG. 7. Splitting of the $1s$ heavy hole and light hole exciton level in $\text{Ga}_{1-x}\text{Mn}_x\text{As}$ as a function of manganese concentration x , assuming a manganese polarization of 100% and using the computed spin polarization from Table II.

The valence band spin-orbit splittings in GaAs (Ref. 15) and in ZnSe (Sec. III A) are roughly one order of magnitude smaller than the values for $N_0\beta$ of Table II, suggesting that the region around 10% manganese concentration will be most interesting. In order to study this region we add the exchange terms of Eqs. (16) and (17), using the exchange constants of Table II, to an eight band $\mathbf{k}\cdot\mathbf{p}$ matrix for GaAs which contains the spin-orbit splitting parameter Δ at the Γ point. The resulting splittings of the valence and conduction band edges are shown in Fig. 6. A 100% manganese polarization is assumed in the calculation. For $x < 0.04$ the exchange interaction between the free carriers and the localized manganese d states can be treated as a perturbation compared to the spin-orbit term. In this concentration regime, the heavy-hole, light-hole degeneracy splits into four states, with equal spacing of $\frac{1}{3}N_0\beta x\langle S \rangle$ between the states. For $x > 0.04$ the exchange interaction starts to dominate over the spin-orbit term and the spin splitting becomes more complicated. On the right side of Fig. 6 we show the optical transitions for circularly polarized light at 10% manganese concentration.

The labels of the light hole and split-off hole states in Fig. 6 are only approximate, since the exchange term mixes these four states. However, our $\mathbf{k}\cdot\mathbf{p}$ calculations show that the states at this manganese concentration retain at least 85% of their original character. We therefore plot in Fig. 7 the heavy hole and light hole $1s$ exciton splitting of $\text{Ga}_{1-x}\text{Mn}_x\text{As}$ as a function of manganese concentration. Note that the light hole exciton splitting is not a linear function of the manganese concentration even within the mean-field approximation as a result of the interplay between spin-orbit coupling and exchange interaction. This needs to be taken into account when extracting exchange constants from experimental data.

Finally we show in Fig. 8 the spin splitting of the valence band edge for $\text{Ga}_{1-x}\text{Mn}_x\text{As}$ as a function of manganese concentration from 0 to 100%, using the same $\mathbf{k}\cdot\mathbf{p}$ Hamiltonian as before. Only the character of the heavy hole states remains unchanged for the entire concentration range. This is due to

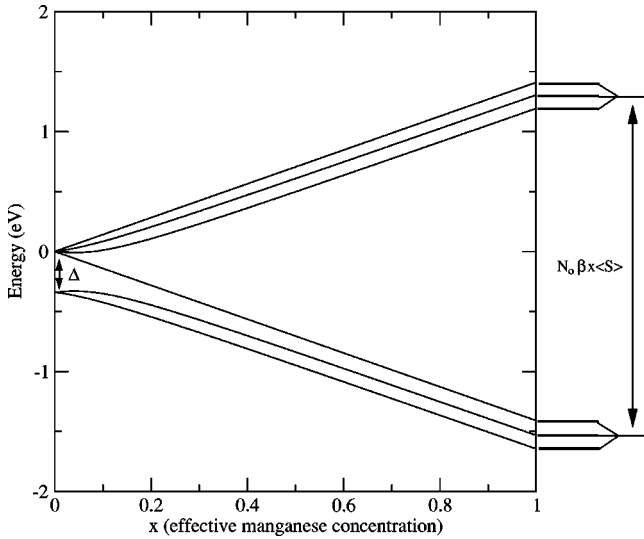


FIG. 8. Splitting of the $\text{Ga}_{1-x}\text{Mn}_x\text{As}$ valence edge as a function of manganese concentration x assuming a manganese polarization of 100% and using the computed spin polarization from Table II. Only the heavy hole states are eigenstates across the entire range of x .

the fact that the spin and orbital part can be separated for these states rendering them eigenstates of the exchange interaction at the same time. Light holes and split-off holes, however, are strongly mixed by the exchange term for high manganese concentrations. The most interesting feature of Fig. 8 in the current context is the spin-orbit splitting of the two spin-split groups of valence bands in the high concentration limit, since the fully relativistic pseudopotential method allows us to obtain these splittings *ab initio*. To first order the splitting of these states is equal to $\frac{1}{3}\Delta$, where Δ is the spin-orbit parameter of GaAs. We therefore expect to see a splitting of approximately 120 meV. The values found by exact diagonalization, shown in Fig. 8, agree with the approximate result to within a few *meV*. The difference arises from second order terms.

D. Fully relativistic pseudopotential results

The fully relativistic pseudopotential method developed in Sec. II of this paper allows us to obtain self-consistent *ab initio* solutions including spin-orbit and exchange coupling. It is particularly interesting to examine whether the valence spin splitting pattern really follows the form suggested by the $\mathbf{k}\cdot\mathbf{p}$ model in the previous section.

As before we will consider here the high concentration limit, i.e., we will study hypothetical ferromagnetic MnAs and MnSe in the zinc blende structure. Assuming the magnetization is along the z axis of the conventional zinc blende unit cell only the tetragonal symmetry operations of Table I are allowed. Hence, in contrast to the scalar-relativistic case, it is necessary to plot the dispersions parallel and perpendicular to the spin-polarization axis.

Figure 9 shows the fully relativistic band structure of ferromagnetic MnAs with points X , U , and K in the plane perpendicular to $[001]$, the direction of magnetization. In Fig.

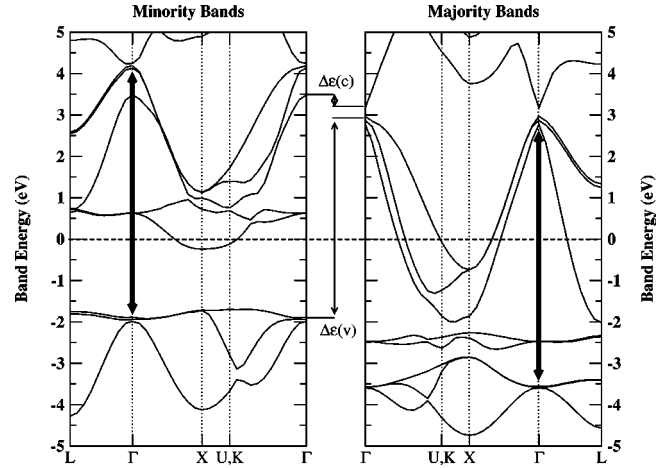


FIG. 9. Relativistic band structure for majority and minority spin states of hypothetical ferromagnetic zinc blende MnAs at a lattice constant of 5.65 Å. The points X , U , and K lie in the plane perpendicular to the direction of magnetization.

10 the same points lie in the plane parallel to the direction of magnetization. Figures 11 and 12 show the dispersions for MnSe along the same Brillouin zone directions.

Compared to the scalar-relativistic case the separation into minority and majority states is a little more subtle. In the fully relativistic case the *expectation value* of the spin along the magnetization axis serves as the label. If for a particular state this expectation value is negative the considered state points *mainly* opposite to the net spin-polarization axis and thus belongs to the minority channel and vice versa.

As expected, spin-orbit coupling does not lead to a drastic modification of the scalar-relativistic band structure of MnAs and MnSe. However, along the directions that lie in the plane parallel to the magnetization axis (Figs. 10 and 12) all the remaining degeneracies in the valence band are lifted. Only along the Γ - X direction perpendicular to the magnetization

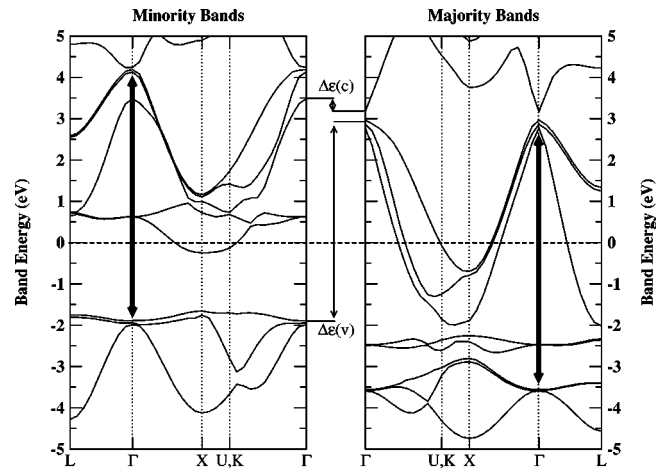


FIG. 10. Relativistic band structure for majority and minority spin states of hypothetical ferromagnetic zinc blende MnAs at a lattice constant of 5.65 Å. The points X , U , and K lie in the plane parallel to the direction of magnetization.

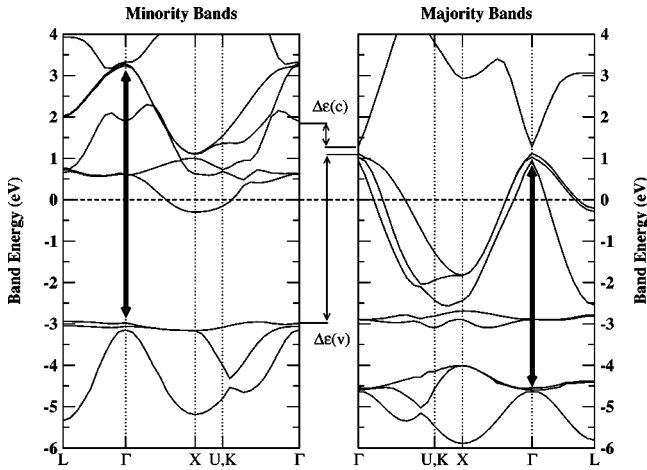


FIG. 11. Relativistic band structure for majority and minority spin states of hypothetical ferromagnetic zinc blende MnSe at a lattice constant of 5.65 Å. The points X, U, and K lie in the plane perpendicular to the direction of magnetization.

axis does the interplay between the \vec{k} dependent spin-orbit interaction and the \vec{k} independent, effective exchange-correlation field $\vec{b}_{xc}(\vec{r})$ lead to an accidental degeneracy of two valence bands.

In this study we are particularly interested in the effect that the spin-orbit coupling term has on the states at the Brillouin zone center. Figure 13 summarizes the relevant information for the MnAs valence band states. The splitting of ± 2.405 eV is that obtained from the scalar-relativistic band structure which led to the valence band exchange constant calculated in Sec. III B and used throughout Sec. III C. The levels of the six exchange and spin-orbit split states are those from our fully relativistic band structure calculation.

We find that the *ab initio* spin-orbit splitting between the majority states is 20 to 30% smaller than that obtained from the $\mathbf{k} \cdot \mathbf{p}$ analysis of Sec. III C, and for the minority states it is

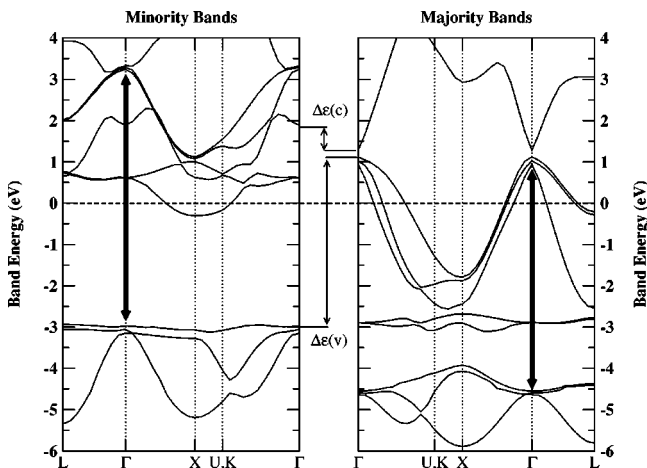


FIG. 12. Relativistic band structure for majority and minority spin states of hypothetical ferromagnetic zinc blende MnSe at a lattice constant of 5.65 Å. The points X, U, and K lie in the plane parallel to the direction of magnetization.

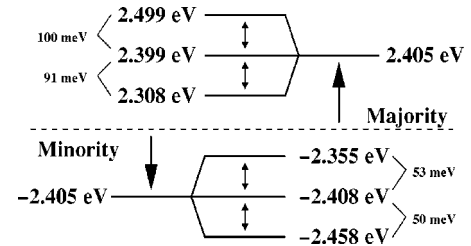


FIG. 13. Schematic of the valence band energy levels at Γ for MnAs.

even 60% below the $\mathbf{k} \cdot \mathbf{p}$ value. The apparent reason for the overestimation by the $\mathbf{k} \cdot \mathbf{p}$ method is that, unlike the pseudopotential calculations here, they are not completely self-consistent. Thus the band structure in the pseudopotential calculation will relax according to the correct filling of the available states. Notice that the majority valence band top lies above the Fermi level, whereas the corresponding minority states are completely occupied.

There is a second difference between the *ab initio* calculations considered here and the model used in Sec. III C. In the model Hamiltonian the interaction between As-*p* and Mn-*d* states was included effectively by a Kondo-like term (15). However, from the density of states plot in Fig. 5 we can see that these states hybridize very strongly. This is particularly true at the Γ point. Since the spin-orbit interaction introduced by manganese is smaller than that arising from arsenic, both results can be reconciled.

Finally we answer the question of how strongly the valence band exchange constant $N_0\beta$ is affected by spin-orbit coupling. Assuming the validity of the Schrieffer-Wolff transformation for spin-dependent potentials there are two ways in which spin-orbit coupling could change the scalar-relativistic result. First the net magnetization could be affected by the self-consistent treatment of spin-orbit coupling. This seems especially plausible because the Fermi level cuts right through strongly *p-d* hybridized, spin-orbit coupled states (see Figs. 9–12). Second, as already discussed, the valence band level splittings will be more complicated in the self-consistent treatment of the problem.

However, we find that the net spin polarizations for MnAs and MnSe are practically unaffected by spin-orbit coupling and we obtain values of $3.44\mu_B$ for MnAs and $4.42\mu_B$ per formula unit for MnSe as in the scalar-relativistic case. In addition, the small shifts of the relativistic exchange splittings discussed in Fig. 13 have only a minor effect on the exchange constants listed in Table III.

TABLE III. Spin-polarization and exchange constants for MnAs and MnSe.

	$ M $ (μ_B)	$N_0\alpha$ (eV)	$N_0\beta$ (eV)
MnAs fully relativistic	3.44	0.18	-2.80
MnSe fully relativistic	4.42	0.28	-1.86

IV. CONCLUSION

We performed scalar-relativistic and fully relativistic band structure calculations for MnAs and MnSe. Spin-orbit coupling lifts the triply degenerate exchange split valence band states at the Γ point and we find that the exact value of this splitting can only be obtained in a completely self-consistent treatment that includes the effect of spin-orbit coupling. Although the spin-orbit splittings are absent in the scalar-relativistic treatment we find that the valence band exchange constants ($N_0\beta$) determined for MnAs and MnSe are unchanged when treated fully relativistically. Thus our results

provide computational support for scalar-relativistic calculations of the conduction and valence band exchange constants in dilute magnetic semiconductors.

ACKNOWLEDGMENTS

This work made use of the MRL Computing Facilities supported through NSF Award No. DMR96-32716. The work was supported by the ONR Grant No. N00014-00-10557, by NSF-DMR under Grant No. 9973076 and by ACS PRF under the grant 33851-G5. G.T. acknowledges support from the MRL, funded by the Corning Foundation.

*Electronic address: theurich@mrl.ucsb.edu

- ¹J.K. Furdyna, J. Appl. Phys. **64**, R29 (1988).
- ²N. Samarth, P. Klosowski, H. Luo, T.M. Giebultowicz, J.K. Furdyna, J.J. Rhyne, B.E. Larson, and N. Otsuka, Phys. Rev. B **44**, 4701 (1991).
- ³S. Sanvito and N.A. Hill, Phys. Rev. B **62**, 15 553 (2000).
- ⁴H. Ohno, A. Shen, F. Matsukura, A. Oiwa, A. Endo, S. Katsumoto, and Y. Iye, Appl. Phys. Lett. **69**, 363 (1996).
- ⁵H. Ohno and F. Matsukura, Solid State Commun. **117**, 179 (2001).
- ⁶H. Ohno, J. Magn. Magn. Mater. **200**, 110 (1999).
- ⁷T. Dietl, H. Ohno, F. Matsukura, J. Cibert, and D. Ferrand, Science **287**, 1019 (2000).
- ⁸M. Abolfath, T. Jungwirth, J. Brum, and A.H. MacDonald, Phys. Rev. B **63**, 054418 (2001).
- ⁹B.E. Larson, K.C. Hass, H. Ehrenreich, and A.E. Carlsson, Phys. Rev. B **37**, 4137 (1988).
- ¹⁰M.I. D'yakonov and V.I. Perel', Sov. Phys. JETP **33**, 1053 (1971).
- ¹¹J. Fabian and S.D. Sarma, J. Vac. Sci. Technol. B **17**, 1708 (1999).
- ¹²T. Moriya, Phys. Rev. **120**, 91 (1960).
- ¹³B.E. Larson and H. Ehrenreich, Phys. Rev. B **39**, 1747 (1989).
- ¹⁴L.M. Sandratskii and J. Kübler, Mod. Phys. Lett. B **10**, 189 (1996).
- ¹⁵G. Theurich and N.A. Hill, Phys. Rev. B **64**, 073106 (2001).
- ¹⁶J. Ihm, A. Zunger, and M.L. Cohen, J. Phys. C **12**, 4409 (1979).
- ¹⁷M.C. Payne, M.P. Teter, D.C. Allan, T.A. Arias, and J.D. Joannopoulos, Rev. Mod. Phys. **64**, 1045 (1992).
- ¹⁸G. Kresse and J. Furthmüller, Comput. Mater. Sci. **6**, 15 (1996).
- ¹⁹T. Sasaki, A.M. Rappe, and S.G. Louie, Phys. Rev. B **52**, 12 760 (1995).
- ²⁰E.G. Moroni, G. Kresse, J. Hafner, and J. Furthmüller, Phys. Rev. B **56**, 15 629 (1997).
- ²¹G.B. Bachelet and M. Schlüter, Phys. Rev. B **25**, 2103 (1982).
- ²²G.B. Bachelet, D.R. Hamann, and M. Schlüter, Phys. Rev. B **26**, 4199 (1982).
- ²³D.R. Hamann, Phys. Rev. B **40**, 2980 (1989).
- ²⁴A.M. Rappe, K.M. Rabe, E. Kaxiras, and J.D. Joannopoulos, Phys. Rev. B **41**, 1227 (1990).
- ²⁵N. Troullier and J.L. Martins, Phys. Rev. B **43**, 1993 (1991).
- ²⁶D. Vanderbilt, Phys. Rev. B **41**, 7892 (1990).
- ²⁷C. Kittel, *Quantum Theory of Solids* (Wiley, New York, 1987).
- ²⁸L. Kleinman, Phys. Rev. B **21**, 2630 (1980).
- ²⁹The SPINOR code is publically available at URL <http://spinor.sourceforge.net/>
- ³⁰L. Kleinman and D.M. Bylander, Phys. Rev. Lett. **48**, 1425 (1982).
- ³¹S.G. Louie, S. Froyen, and M.L. Cohen, Phys. Rev. B **26**, 1738 (1982).
- ³²P. Hohenberg and W. Kohn, Phys. Rev. **136**, B864 (1964).
- ³³W. Kohn and L. Sham, Phys. Rev. **140**, A1133 (1965).
- ³⁴U. von Barth and L. Hedin, J. Phys. C **5**, 1629 (1972).
- ³⁵L. Nordström and D.J. Singh, Phys. Rev. Lett. **76**, 4420 (1996).
- ³⁶W.E. Pickett, J. Korean Phys. Soc. **23**, S70 (1996).
- ³⁷J.P. Perdew and A. Zunger, Phys. Rev. B **23**, 5048 (1981).
- ³⁸H.J. Monkhorst and J.D. Pack, Phys. Rev. B **13**, 5188 (1976).
- ³⁹L.M. Sandratskii, Sov. Phys. J. **9**, 941 (1979).
- ⁴⁰A. Messiah, *Quantum Mechanics II* (North-Holland, Amsterdam, 1965).
- ⁴¹E. Wigner, *Group Theory and Its Application to the Quantum Mechanics of Atomic Spectra* (Academic Press, New York, 1959).
- ⁴²P. Klosowski, T.M. Giebultowicz, J.J. Rhyne, N. Samarth, H. Luo, and J.K. Furdyna, J. Appl. Phys. **70**, 6221 (1991).
- ⁴³J.R. Chelikowsky and M.L. Cohen, Phys. Rev. B **14**, 556 (1976).
- ⁴⁴J.P. Walter, M.L. Cohen, Y. Petroff, and M. Balkanski, Phys. Rev. B **1**, 2661 (1970).
- ⁴⁵A. Ebina, M. Yamamoto, and T. Takahashi, Phys. Rev. B **6**, 3786 (1972).
- ⁴⁶G.B. Bachelet and N.E. Christensen, Phys. Rev. B **31**, 879 (1985).
- ⁴⁷J.R. Schrieffer and P.A. Wolff, Phys. Rev. **149**, 491 (1966).
- ⁴⁸S. Sanvito, P. Ordejon, and N.A. Hill, Phys. Rev. B **63**, 165206 (2001).